SUGISAKA MASANORI

Journal of Advances in Artificial Life Robotics
Vol. 1(1); June (2020), pp. 27–34
ON LINE ISSN 2435-8061; ISSN-L 2435-8061
https://alife-robotics.org/jallr.html

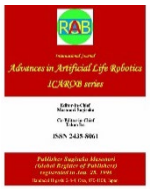

Research Article

Parallel Full-Wave Electromagnetic Field Analysis Using Anatomical Human Body Models

Amane Takei, Makoto Sakamoto
Department of Electrical and System Engineering, University of Miyazaki, 1-1 Gakuen Kibanadai-Nishi, Miyazaki, 889-2192, Japan

ARTICLE INFO

Article History

Received 24 November 2019
Accepted 10 July 2020

Keywords

Iterative domain decomposition method
Parallel finite element method
Berenger's PML
Large-scale analysis
Microwave analysis

ABSTRACT

The authors have investigated a high-accuracy analysis for the electromagnetic field of anatomical human body models using the parallel finite element method. In the full-wave electromagnetic field analysis by the parallel finite element analysis with anatomical human models, efficient conversion from voxels to finite element meshes and speed-up of an analysis become important topics. In this paper, we propose parallel mesh generation method with mesh smoothing, and show to be able to generate large-scale mesh very effective. Then, we evaluated the performance of two kinds of iterative method by numerical experiments using large-scale human body model. As the results, the COCR method is very useful as the interface solver in the DDM for high-frequency electromagnetic field analysis using anatomical human model.

1. Introduction

Recently, a numerical electromagnetic analysis using anatomical human model from CT/MRI is required strongly[1],[2]. Important topics in numerical electromagnetic field analysis using numerical human body model are efficient conversion from voxels to finite element meshes and speed-up of analyses.

In our research group, we are investigating and developing a full-wave electromagnetic analysis method for large-scale analysis that has several hundred million meshes based on the parallel finite element method [3]. To apply the parallel finite element analysis code in the computation using the anatomical human model, a parallel mesh generation algorithm and a mesh smoothing function are verified in the viewpoint of accuracy and performances using a super computer system.

On the other hand, the high-frequency electromagnetic problem with our formulation is complex symmetric, and we have employed the conjugate orthogonal conjugate gradient (COCG) method for the interface problem. However, because of the ill-conditioned coefficient matrix of the large-scale analysis, it suffers from low convergence rate. To solve this issue, we propose a domain decomposition method (DDM) algorithm based on the conjugate orthogonal conjugate residual (COCR) method [4]. As shown in this paper, in order to verify the accuracy of the developed analytical solver, we calculate TEAM Workshop #29, which is a benchmark problem, and evaluate the accuracy of the analytical solver. Moreover, an improvement of the performance by using COCR method with huge-scale anatomical human model that has 1,700 million meshes is revolutionary in huge-scale analyses.

2. Formulations

Corresponding author's E-mail: takei@cc.miyazaki-u.ac.jp, URL: www.miyazaki-u.ac.jp/english/

2.1. *Governing equations*

Let Ω be a domain with a boundary $\partial\Omega$. The vector wave equations [5] that describe an electromagnetic field with a single angular frequency ω (rad/s) are derived from Maxwell's equations containing the displacement current. The vector wave equations describing an electric field $\mathbf{E}$ (V/m) are given by Eqs. (1a)-(1c) for a current density $\mathbf{J}$ (A/m^2) with j as an imaginary unit:

$$\text{curl}\left(\frac{1}{\mu}\,\text{curl}\,\mathbf{E}\right) - \omega^2\varepsilon\mathbf{E} - j\omega\sigma\mathbf{E} = j\omega\,\mathbf{J} \quad \text{in } \Omega\,, \tag{1a}$$

$$\mathbf{E}\times\mathbf{n} = \mathbf{0} \quad \text{on } \partial\Omega\,, \tag{1b}$$

Permittivity and permeability are given by ε (F/m) and μ (H/m), respectively. By solving Eq. (1a) under the essential boundary condition in (1b), the electric field $\mathbf{E}$ is calculated.

Magnetic fields are calculated by a post-process using Faraday's law of induction, which is expressed by Eq. (2).

$$\text{rot}\mathbf{E} - j\omega\mu\mathbf{H} = \mathbf{0} \tag{2}$$

2.2. *Finite element formulation*

Here, we describe the finite element discretization. The electric field E is approximated with Nédélec elements (edge elements). The finite element approximation is performed as follows.

Find $\mathbf{E}_\text{h}$ such that

$$\iiint_\Omega (1/\mu)\text{rot}\mathbf{E}_\mathbf{h}\cdot\text{rot}\mathbf{E}_\mathbf{h}^*\,dv - \omega^2\iiint_\Omega \varepsilon\mathbf{E}_\mathbf{h}\cdot\mathbf{E}_\mathbf{h}^*\,dv = j\omega\iiint_\Omega \mathbf{J}_\mathbf{h}\cdot\mathbf{E}_\mathbf{h}^*\,dv. \tag{3}$$

Here, $\mathbf{J}_\text{h}$ is an electric current density approximated by the conventional piecewise linear tetrahedral elements.

3. Parallel algorithms for solving large linear system

3.1. *Domain decomposition method*

The domain decomposition method (DDM) is introduced to high-frequency problems using the E method. Let us put the finite element equations of (3) in matrix form, as follows:

$$Ku = f, \tag{4}$$

where K denotes the coefficient matrix, u the unknown vector, and f the known right-hand side vector. As shown in the following equation, the domain Ω is decomposed into N pieces so that there is no overlap in the boundary between subdomains, namely

$$\Omega = \bigcup_{i=1}^{N} \Omega^{(i)}. \tag{5}$$

After domain decomposition, (4) is rewritten as follows:

$$\begin{bmatrix} K_{II}^{(1)} & & \cdots & 0 & K_{IB}^{(1)}R_B^{(1)} \\ 00 & \ddots & & \vdots & \vdots \\ \vdots & & \ddots & 0 & \vdots \\ 0 & \cdots & 0 & K_{II}^{(N)} & K_{IB}^{(N)}R_B^{(N)} \\ R_B^{(1)T}K_{IB}^{(1)T} & \cdots & \cdots & R_B^{(N)T}K_{IB}^{(N)T} & \sum_{i=1}^{N} R_B^{(i)T}K_{BB}^{(i)}R_B^{(i)} \end{bmatrix} \begin{bmatrix} u_I^{(1)} \\ \vdots \\ \vdots \\ u_I^{(N)} \\ u_B \end{bmatrix} = \begin{bmatrix} f_I^{(1)} \\ \vdots \\ \vdots \\ f_I^{(N)} \\ f_B \end{bmatrix} \tag{6}$$

where the subscripts I and B correspond to unknowns in the interior of subdomains and on the interface boundary, respectively. $R_B^{(i)}$ maps the global degrees of freedom (DOF) of the interface onto the local DOF of the subdomain interface. Equation (6) leads to linear systems as follows:

$$K_{II}^{(i)}u_I^{(i)} = f_I^{(i)} - K_{IB}^{(i)}R_B^{(i)}u_B\,,\ i = 1,\ldots,N\,, \tag{7}$$

$$S\,u_B = g\,, \tag{8}$$

$$S = \sum_{i=1}^{N} R_B^{(i)T}S^{(i)}R_B^{(i)}\,,$$
$$S^{(i)} = K_{BB}^{(i)} - K_{IB}^{(i)T}\left(K_{II}^{(i)}\right)^{-1}K_{IB}^{(i)}, \tag{9}$$

$$g = \sum_{i=1}^{N} R_B^{(i)T}g^{(i)},$$
$$g^{(i)} = f_B^{(i)} - K_{IB}^{(i)T}\left(K_{II}^{(i)}\right)^{-1}f_I^{(i)}\,. \tag{10}$$

We call (7) the subdomain problems, (8) the interface problem, S the Schur complement matrix. In this paper,

(7) are solved by the direct method based on Gaussian elimination, on the other hand, (8) is solved by the iterative methods. Here, the Krylov subspace methods require the coefficient matrix-vector multiplication in each iterative procedure, however, such calculation for (8) can be replaced by likely solving subdomain problems. Therefore, in our DDM algorithm, subdomain problems are also solved at each iteration for solving the interface problem.

3.2. *COCG method*

In this paper, we introduce two kinds of iterative methods for the subdomain problems and the interface problem. Firstly, Fig. 1 shows the preconditioned COCG method. In Fig.1, M is the preconditioning matrix, $(x, y) = \sum_{i=1}^{m} \bar{x}_i y_i$ an inner product of complex vectors x and y, $\|\cdot\|$ the Euclidean norm, and δ a positive constant as the convergence criterion.

u_B^0 : an initial guess
$r^0 = g - Su_B^0$
$z^0 = M^{-1}r^0$
$p^0 = z^0$
$for\ n = 0,1, \ldots$
$q^n = Sp^n$
$\alpha^n = (\bar{r}^n, z^n)/(\bar{p}^n, q^n)$
$u_B^{n+1} = u_B^n + \alpha^n p^n$
$r^{n+1} = r^n - \alpha^n q^n$
$if\ (\|r^{n+1}\|/\|r^0\| < \delta)\ break;$
$z^{n+1} = M^{-1}r^{n+1}$
$\beta^n = (\bar{r}^{n+1}, z^{n+1})/(\bar{r}^n, z^n)$
$p^{n+1} = z^{n+1} + \beta^n p^n$

Fig. 1. Algorithm of preconditioned COCG method.

3.3. *COCR method*

The preconditioned COCR method [4] is shown in Fig. 2. [6] The COCR method requires more or less the same amount of computational cost and working memory per iteration as the COCG method, and is expected to get smooth convergence behavior compared with the COCG method. In particular, the COCR method for (8) has more effect than the COCG method in a large-scale analysis.

u_B^0 : an initial guess
$r^0 = g - Su_B^0$
$t^0 = M^{-1}r^0$
$p^{-1} = 0,\ q^{-1} = 0,\ \beta^{-1} = 0$
$s^0 = St^0$
$for\ n = 0,1, \ldots$
$p^n = t^n + \beta^{n-1}p^{n-1}$
$q^n = Sp^n = s^n + \beta^{n-1}q^{n-1}$
$w^n = M^{-1}q^n$
$\alpha^n = (\bar{t}^n, s^n)/(\bar{q}^n, w^n)$
$u_B^{n+1} = u_B^n + \alpha^n p^n$
$t^{n+1} = t^n - \alpha^n w^n$
$if\ (\|r^{n+1}\|/\|r^0\| < \delta)\ break;$
$s^{n+1} = St^{n+1}$
$\beta^n = (\bar{t}^{n+1}, s^{n+1})/(\bar{t}^n, s^n)$

Fig. 2. Algorithm of preconditioned COCR method.

4. Accuracy verification

4.1. *TEAM29*

We analyze TEAM Workshop #29[8] in order to verify the accuracy of the developed analytical solver.[2] TEAM 29 is a benchmark problem and involves a resonator model.

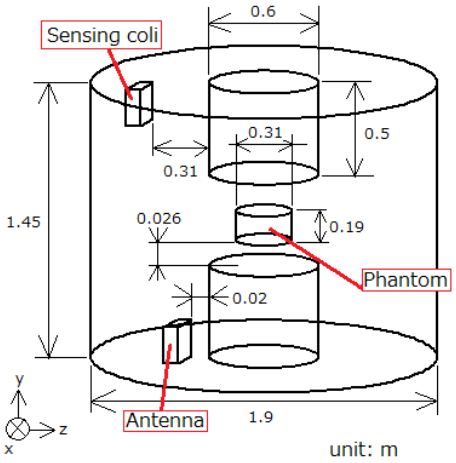

Fig. 3. TEAM 29 cavity resonator model.

Table 1. TEAM 29 model data.

No. of Elements	DOFs	No. of Subdomains
121,277	149,668	100×7

The resonator is cylindrical and has a diameter of 1.9 [m] and a height of 1.45 [m]. In the analysis, a dielectric phantom having a relative permittivity ε_r of 80 and an electric conductivity σ of 0.52 [S/m] is positioned, and the resonance state is investigated. The analysis domain

boundary is a perfect conductor. The analysis model is shown in Fig. 3. Table 1 shows the specifications of the TEAM 29 model. The highest calculation efficiency is achieved when the number of elements contained in one subdomain is approximately 170, and the number of partial domains is determined such that the number of elements contained in one subdomain is equal to 170.

4.2. *Frequency response analysis*

The results of the analysis of TEAM 29 are subjected to frequency response analysis in order to confirm the accuracy of the developed analytical solver. In order to detect the resonant frequency and compare solutions with actual measurements, the frequencies of some range are analyzed. The frequency band of 60 [MHz] to 140 [MHz] is calculated for 2-MHz steps, and the response for every frequency step is investigated. In addition, calculations near the resonance frequency are performed in 0.4-MHz intervals. The computing environment used in the present study is a 25-PC cluster equipped with Intel Core i7-2600K multi-core CPUs (total: 100 cores) and 32 GB memory is used. The compiler used is the gcc. In addition, Message Passing Interface (MPI) is used for the parallelization library. The average calculation time per frequency step and the averagely used memory are shown in Table 2. Fig. 4 shows the frequency response of the magnetic field. The measured and calculated values are shown in Table 3.

Table 2. Specifications of the TEAM 29 model.

No. of Elements	DOFs	No. of Subdomains
121,277	149,668	100×7

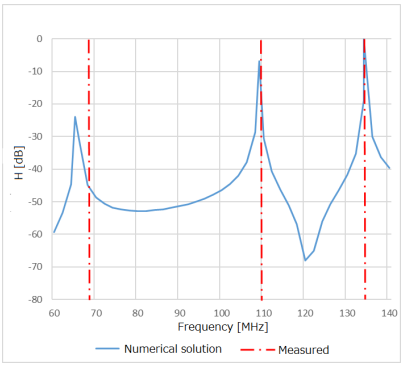

Fig. 4. Numerical and measured frequency response analysis results.

Table 3. Resonance frequencies. (Units: [MHz]. The error rate [%] between measured data and the numerical solution is shown in parentheses.)

Resonance mode	Measured data	FDTD 25-mm mesh	Result
1st	68.6	67 (2.33)	65.6 (4.37)
2nd	110	110	109.0 (0.91)
3rd	134	134	134.4 (0.30)

As shown in Fig. 4, a solution resonating around the resonance frequency of the actually measured value is obtained. In the comparison of the measured and calculated values, the error rate is 4.37 [%] in the 1st mode, 0.91 [%] in the 2nd mode, and 0.30 [%] in the 3rd mode. As the mode increases, the error rate decreases. However, it is the same tendency as the analysis result obtained by the FDTD method. Moreover, the error rate is less than 5 [%], and a solution with high accuracy is obtained.

Therefore, the solution obtained by the developed solver is proven to have a sufficiently high accuracy. Moreover, in the analysis of the dipole antenna applying the PML described in the following sections, the error tolerance index is defined as 5 [%] in order to evaluate the accuracy.

5. Pre-processing

5.1. *Mesh generation and smoothing*

In many numerical human body models employ a binary data format wherein types of organs (including air area) are encoded using voxels. In NICT model[1], the size of the adult male model is 320 voxels wide, 160 voxels deep, and 866 voxels high. Represented as the “char” type, it occupies 44,339,200 bytes of memory. In this research, each voxel is divided into five tetrahedra.

Fig. 5 shows a parallel procedure for generating the domain decomposed mesh. Firstly, the voxel mesh of the numerical human body model is read. Secondly, using ParMETIS [7], the input voxel data is divided into a number of *parts*. After *part* decomposition, all processes can perform remaining procedures independently without communication.

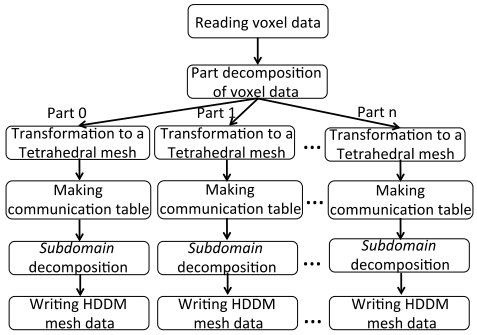

Fig. 5. Procedure for generation of the domain decomposed mesh.

A mesh smoothing technique based on the marching cube-like algorithm is employed in part of the transformation from voxels to tetrahedras of our mesh generation procedure. Fig. 6 shows the schematic of the mesh smoothing. The dotted line (A) in Fig. 6 shows the original boundary between different materials. Firstly, the boundary is smoothed by triangular prisms, as shown by the dashed line (B). This is referred to as one-level smoothing. Next, by searching for angles of 45 degrees, the points on the angles are moved so that these angles become 0 degrees, as shown by (C). The solid line (D) shows the smoothed boundary obtained by these two-level smoothing operations.

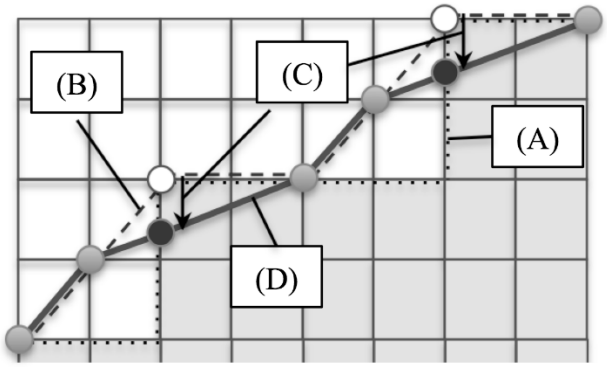

Fig. 6. Schematic of the mesh smoothing.

5.2. *Performance evaluation*

First, accuracy verification for mesh smoothing is performed using the voxel mesh model of TEAM 29. An accuracy verification is performed using this smoothed model. The processing time necessary to smoothing is less than 1 second. To detect the resonant frequency and compare solutions with actual measurements, the resonance state is investigated. The frequency band of 60–70 MHz is calculated for 0.4 MHz steps around resonant frequencies, and the response for every frequency step is investigated. Computations are performed using 1,152 cores (72 nodes) of the FX10 supercomputer. A comparison between measured resonant frequencies [8] is shown in Table 4. Resonances do not occur in the frequency band of 60–70 MHz using the original voxel mesh and the one-level smoothing mesh. On the other hand, the obtained solution is in very good agreement with that obtained using the two-level smoothing. The maximum error rate between the obtained solution and the measurement is 6.10% in the mode.

Table 4. Resonant frequencies in MHz.(( ): error rate between Measured Data (68.6 MHz) and Numerical Solutions (%))

Smoothing type	Result
None (Original voxel model)	N/A
One-level smoothing	N/A
Two-level smoothing	64.4 (6.10)

Fig. 7 shows conditions of the analysis model. The dipole antenna is set above the breast. The distance between the breast and antenna H is 0.06 m. The antenna length L is 0.5 m, which is same as half wavelength at 300 MHz. The lengths of the model's sides are x = 0.64 m, y = 0.32 m, and z = 1.732 m. [6]

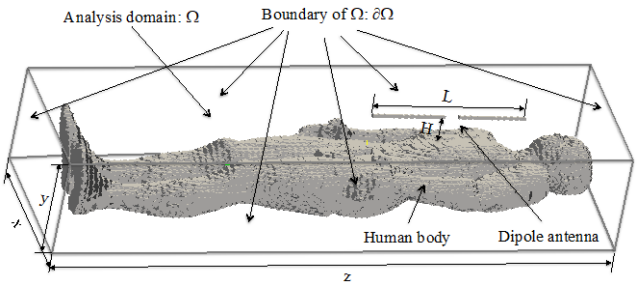

Fig. 7. Conditions of the analysis model.

Table 5 show the generation conditions and elapsed times of the HDD mesh using 12-nodes (96-cores) on the FX10. In this paper, full body models of tetrahedral elements are generated from 4mm voxel models. Models "1, 2, 3, 4 and 5" shown in Table 5 with 27.71 million tetrahedral elements are obtained from the 4mm voxel model.

The mesh decomposition tool used in this research is designed to add the voxel partition function to ADVENTURE Metis [9]. As shown in Table 5, the longest calculation time is spent on the part and subdomain decompositions. It is difficult to reduce the calculation cost of the part and subdomain decompositions with largest calculation cost in the

original ADVENTURE Metis. However, since communication among nodes in the subdomain decomposition is not required, the calculation time can be reduced by increasing the number of nodes. On the other hand, the calculation times for the transformation of the voxel data to a tetrahedral mesh and the communication table generation represent only a small part of the overall calculation time and the large-scale initial mesh generation is not required in advance. These figures of merit demonstrate that the developed function is very effective.

Table 5. Generation conditions and elapsed time for the HDD mesh of 4mm.

Model	Num. of parts	Num. of doms /part	Total (sec)	Part decomp-osition (sec)	Tetra & Com. table (sec)	Subdomain decomposition (sec)
1	300	1000	50.12	20.02	0.09	15.25
2	600	500	40.64	21.77	0.08	8.85
3	1200	250	40.21	23.78	0.08	8.37
4	2400	125	41.35	26.20	0.09	5.85
5	4800	62	44.21	30.23	0.11	5.83

6. Numerical experiments

6.1. *Performance evaluation*

The electromagnetic field in the human body is analyzed via refined meshes of Model 1 in Tables 3. All computations are performed using Oakleaf-FX10 supercomputer at the University of Tokyo. We analyzed frequencies of 1 (MHz), 8 (MHz), 70 (MHz) and 300 (MHz) using the full-wave electromagnetic field analysis based on the DDM. The electromagnetic field source is a dipole antenna assumed to have a current source of 0.8 (A). In the analyses using NICT numeric human body models, it is necessary for the user to provide the electric conductivity and the permittivity of the material ID for each internal organ. Electric conductivities and relative permittivities given to internal organs. These physical values are based on the human organs property database for computational biomechanics open to the public by the Institute of Physical and Chemical Research (RIKEN) in Japan [10].

6.2. *Performance evaluation*

Full-wave electromagnetic analyses [11] are performed using the 2mm model that is refined Model1 once. The model has 220 million tetrahedral elements. Computations are performed using 75-nodes (150 processes x 8 threads) of the Oakleaf-FX10. The iteration count and calculation time for each frequency comparing COCG method and COCR method are shown in Table 6.

The number of iterations required by the DDM is largest for the lowest frequency (1 MHz) in each iterative method. Generally, the matrix equation becomes semi-definite in the full-wave electromagnetic analysis based on the vector wave equation. However, when the frequency becomes lower, the matrix equation becomes non-definite. Both results indicate this thing. Fig. 8 shows convergence histories in case of 1 (MHz) using 2mm model. As a result, the iterative calculation is improved drastically by using COCR method as interface solver in DDM. In the previous research by Sogabe and Chou, COCR method solves the matrix which size is 2,534 x 2,534[4]. In this result, the number of iteration is reduced from the result by using COCG method. On the other hand, more conspicuous improvement is seen by using COCR method in the interface problem with the anatomical human model.

Then, to confirm performances of the huge-scale analysis, the analyses in the smallest frequency are performed using 1mm model that is refined Model1 twice as the most difficult case of the computation. The model has 1,760 million tetrahedral elements. Computations are performed using 600-nodes (1,200 processes x 8 threads) of the Oakleaf-FX10. The iteration count and calculation time in 1 MHz comparing COCG method and COCR method are shown in Table 7. Fig. 9 shows convergence histories. We succeed calculation using huge-scale model that has 1,760 million tetrahedral elements. The iterative calculation is also improved by using COCR method in this case.

Table 6. Numerical result using 2mm Model.

Frequency (MHz)	Iter. method	Num. of Iter.	Time (sec)	Peak (%)
1	COCG	13,798	10,330	4.97
	COCR	477	465	3.86
8	COCG	1,383	1,107	4.65
	COCR	221	278	3.02
70	COCG	793	675	4.38
	COCR	128	197	2.50
300	COCG	747	628	4.43
	COCR	86	160	2.09

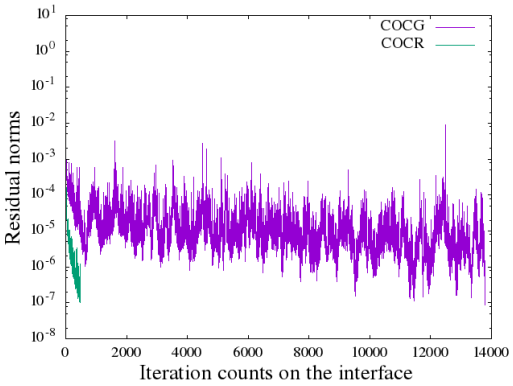

Fig. 8. Convergence histories in case of 1 MHz using 2mm model from once refined MODEL1.

Table 7. Numerical result using 1mm model.

Frequency (MHz)	Iter. method	Num. of Iter.	Time (sec)	Peak (%)
1	COCG	7,348	7,071	4.37
	COCR	1,189	1,319	3.82

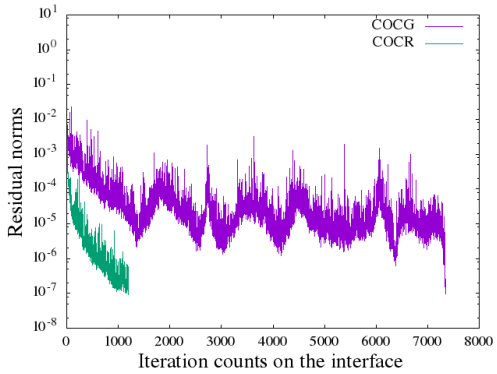

Fig. 9. Convergence histories in case of 1 MHz using 1mm model from twice refined MODEL1.

7. Conclusion

In this paper, we propose parallel mesh generation method with mesh smoothing, and show to be able to generate large-scale mesh very effective. Then, we evaluated the performance of two kinds of iterative method by numerical experiments using large-scale human body model. As the results, selecting iterative method is very important for high-frequency electromagnetic field analysis using anatomical human model. The COCR method is expected to reduce both iteration counts and computation time compared to the COCG method in the analysis using huge-scale human body model.

Acknowledgment

This work was supported by JSPS KAKENHI Grant Number JP17H03256, JP17H02829, JP18KK0278, JP19H01098

References

1. NICT EMC group home page: http://emc.nict.go.jp/bio/index.html
2. E. Conil, A. Hadjem, F. Lacroux, M. F. Wong, and J. Wiart, "Variability analysis of SAR from 20 MHz to 2.4 GHz for different adult and child models using finite-difference time-domain, " Phys. Med. Biol., vol.53, no.6, pp.1511–1525 (2008)
3. A. Takei, K. Murotani, S. Sugimoto, M. Ogino and H. Kawai, "High-accuracy electromagnetic field simulation using numerical human body models", IEEE Trans. Magn., vol. 52, no. 3 (2016)
4. T. Sogabe and S.L. Zhang, "A COCR method for solving complex symmetric linear systems"s, J. Comput. Appl. Math., vol.199, no.2, pp.297-303 (2007)
5. A. Takei, K. Murotani, S. Sugimoto, M. Ogino, T. Yamada, S. Yoshimura "Performance evaluation of parallel finite element electromagnetic field analysis using numerical human models," JASSE, vol.1, no.1, pp.127-140 (2014)
6. A. Takei, M. Ogino, S. Sugimoto," High-frequency electromagnetic field analysis by COCR method using anatomical human body models," IEEE Transactions on Magnetics, vol. 54, no. 3 (2018)
7. G. Karypis, V. Kumar, "A fast and highly quality multilevel scheme for partitioning irregular graphs", SIAM Journal on Scientific Computing, vol.20, no.1, pp. 359-392 (1998)
8. Y. Kanai, "Description of TEAM workshop problem 29: while body cavity resonator", Tech. Rep. TEAM Workshop in Tucson (1998)
9. K. Murotani, S. Sugimoto, H. Kawai and S. Yoshimura, "Hierarchical domain decomposer with parallel mesh refinement function for billions of DOF scales finite element analysis analyses," International Journal of Computational Methods, vol. 11, no.4 (2014)
10. The human organs property database for computational biomechanics in Institute of Physical and Chemical Research (RIKEN) Home page : http://cfd-duo.riken.go.jp/cbms-mp/index.htm
11. M. Ogino, A. Takei, N. Notsu, S. Sugimoto and S. Yoshimura, "Finite element analysis of high frequency electromagnetic fields using a domain decomposition method based on the COCR method", Theor. Appl. Mech., vol.61, pp.173-181 (2013)

Authors Introduction

Prof. Amane Takei

Amane Takei is working as Associate Professor for Department of Electrical and systems Engineering, University of Miyazaki, Japan. His research interest includes high performance computing for computational electromagnetism, iterative methods for the solution of sparse linear systems, domain decomposition methods for large-scale problems. Prof. Takei is a member of IEEE, an expert advisor of The Institute of Electronics, Information and Communication Engineers (IEICE), a delegate of the Kyushu branch of Institute of Electrical Engineers of Japan (IEEJ), a director of Japan Society for Simulation Technology (JSST).

Prof. Makoto Sakamoto

Makoto Sakamoto received the Ph.D. degree in computer science and systems engineering from Yamaguchi University. He is presently an associate professor in the Faculty of Engineering, University of Miyazaki. He is a theoretical computer scientist, and his current main research interests are automata theory, languages and computation. He is also interested in digital geometry, digital image processing, computer vision, computer graphics, virtual reality, augmented reality, entertainment computing, complex systems and so on.